Novel Functionalized Cellulose Derivatives Fabricated with Cu Nanoparticle: Synthesis, Characterization and Degradation of Organic Pollutants

Faiza Lughmani
NUST: National University of Sciences and Technology
Farzana Nazir
NUST: National University of Sciences and Technology
Shahid Ali Khan
University of Sawabi
Mudassir Iqbal (mudassir.iqbal@sns.nust.edu.pk)
NUST: National University of Sciences and Technology https://orcid.org/0000-0002-9830-8235

Research Article

Keywords: Cellulose derivatives, Cu Nanoparticles, Degradation, Organic pollutants

Posted Date: April 30th, 2021

DOI: https://doi.org/10.21203/rs.3.rs-382606/v1

Version of Record: A version of this preprint was published at Cellulose on January 11th, 2022. See the published version at https://doi.org/10.1007/s10570-021-04388-3.

Abstract

In this study, microcrystalline cellulose (MCC) was modified to oxidized cellulose (OC), 6-deoxycellulose hydrazide and 6-deoxycellulose(N,N-diethyl)amine (MCC-Hyd and MCC-DEM) derivatives and employed as supporting material for the synthesis of copper nanoparticles (NPs). Copper ions from aqueous solution were adsorbed and then reduced to zero valent copper (ZVC) NPs using sodium borohydride on films of prepared derivatives. The characterization of prepared derivatives and Cu NPs embedded films was performed using Fourier Transform Infrared Spectroscopy (FT-IR), Elemental analysis, X-ray diffraction (XRD), Scanning Electron Microscopy (SEM) and Nuclear Magnetic Resonance (NMR) spectroscopy. Ultraviolet/Visible (UV-VIS) spectroscopy was performed for the degradation studies of 4-nitrophenol (4-NP) and various azo dyes *viz.* Congo Red (CR), Methylene Blue (MB), and Methyl orange (MO). Results revealed that all the films showed degradation only in the presence of ZVC NPs. Oxidized cellulose, MCC-Hyd and MCC-DEM showed excellent degradation efficiencies (> 85%) in all the cases. Our findings revealed that MCC derivatives could be efficient and renewable candidates for removal of water pollutants in future.

1. Introduction

Pollution in its all form, is a severe menace to the human health [1].Water pollution causes diarrhea, cholera, malaria, dengue, typhoid, HIV/AIDS [2]. Air pollution releases many hazardous gases like carbon dioxide, carbon monoxide, sulfur oxides and chlorofluorocarbons which cause asthma, lungs cancer [3], and tuberculosis etc. High usage of fertilizers, pesticides, herbicides, and radioactive elements are causing land pollution. Industrial wastes containing textile dyes, paints, and other hazardous detergents, when released unprocessed, cause many serious health issues like cancer, kidney, liver, and skin diseases. Industries like textile, plastics and pigments, pharmaceuticals, and cosmetics are extensively taking advantage of phenolic compounds and dyes for coloring purposes. Colored effluent from these industries is taken as a momentous source of environmental contamination [4, 5]. More than 100,000 commercially available dyes are extensively utilized by these industries. Annual production of synthetic dyes worldwide is over 0.7 million tons [6-8]. Approx. 15% of dye is lost in the course of dyeing process and is released unprocessed to the environment in the form of industrial waste [7, 9], which has serious effects on color and quality of water. It also affects the human health as well as aquatic life. Owing to the scenario cited above, it has become highly mandatory to remove these dyes and pesticides from wastewater to avoid unwanted serious consequences.

Therefore, effective strategies are required for the treatment of organic waste in order to eradicate, or at least minimize the quantity of toxic substances from wastewater. Various techniques presently being employed to eliminate colored chemicals and hazardous metals are electrochemical treatment, filtration, precipitation, osmosis, flotation, coagulation, flocculation, and adsorption [10-15]. The major hindrance in attaining the achievement of physical methods is the limitation associated with, such as expense, possibility of secondary pollutants formation, and partial treatment. Hence there is a dire need to focus on the development of methods that may completely transform organic pollutants, especially with the assistance of an efficient catalyst.

Applications of metallic nanoparticles in various areas have gained growing attention in recent times. These includes sensing, drug delivery, bio-imaging and antibacterial coating [16]. They have also been employed in

different reactions involving coupling, electrochemical, and oxidation and reduction reactions [17]. Metallic nanoparticles are widely employed catalysts for the degradation of organic pollutants, because of larger surface area, catalytic efficiency, easy production, and selectivity for reactions.

However, the low stability of most abundantly available metallic nanoparticles restricts the actual environmental applications in contrast to noble metals which exhibit more stable nanoparticles. For example, copper nanoparticles are highly susceptible to air and under ordinary circumstances are quickly oxidized, that may restrict their practical applications. In the same conditions, nickel nanoparticles also tend to be unstable in the air [18-20]. Other problems associated with use of nanoparticles are agglomeration and separation. Because of extremely small size, it is very difficult to separate these from reaction mixture. Agglomeration occurs because of van der Waals interactions, causing reduction of surface area and resulting in decreases of catalytic efficiency [21]. Therefore, to overcome these limitations in using metallic nanoparticles, it requires support material to achieve effective catalytic activity [22]. These supporting materials may reduce the efficiency to some extent, as a consequence of their relatively small surface area, which ultimately leads to poor accessibility of catalyst towards the reacting species [23, 24].

So active and compelling materials are desired to bring about stability, easy separation, enhanced catalytic activity and reusability [25-27]. As per literature, polymer hybrids and composites are the materials being extensively used to support metallic nanoparticles. e.g. copper nanoparticles incorporated on chitosan-coated cellulose microfiber mats (CS-CMM) as catalyst were employed for the reduction studies of 4NP, 2NP and cresyl blue dye [22]. Reduction of thymol violet using TiO_2/Cs-CMM catalyst was also carried out, reaction equilibrium was attained in 90 minutes [28]. Au nanoparticles embedded in poly(AMPS-co-HEMA) composites were used for selective reduction of nitrophenols and reduction occurred in 20 minutes [29]. Cellulose acetate fibers loaded with silver nanoparticles were studied for conversion of 2,4-dinitrophenol [30].

Cellulose is natural, most pervasive, renewable, and highly abundant organic polymer. It is non-toxic, colorless and odorless with auspicious qualities e.g. biocompatibility, thermal stabilization, hydrophilicity, excellent mechanical strength etc. however cellulose in its pure form has low or no adsorption capacity [22, 23, 31-33].

The degradation of the dyes is well recognized reductive cleavage of azo group. Being a good electron donor, degradation reaction occurs on the surface of metal. The azo dyes molecules accept electrons from metal and transfer into transitional products when combining with H^+ [34]. Different reaction schemes and mechanism have been proposed and studied in this regard [27, 34, 35]. Proposed degradation mechanism is given below. (Figure 1)

In this study degradation of some of the selected toxic dyes like 4-nitrophenol (4-NP) and various azo dyes (Congo Red (CR), Methylene Blue (MB), and Methyl orange (MO)) using zerovalent copper nanoparticles incorporated in MCC and functionalized MCC films has been studied. MCC was functionalized with the aim to eradicate dye effluents from wastewater. The acid and amino groups in functionalized MCC helps high uptake of Cu(II) ions possibly due to presence of more adsorption sites for metals ions and in binding dye molecules, thus improving adsorption process.

2. Materials And Methods

2.1 Materials

All chemicals and reagents, *viz.* Microcrystalline cellulose (MCC) (DAEJUNG 20–100 um), Nitric acid (HNO_3) (Sigma Aldrich), Phosphoric acid (H_3PO_4) (Sigma Aldrich), Sodium nitrite ($NaNO_2$) (Sigma Aldrich), Sulphuric acid (H_2SO_4) (Sigma Aldrich), Sodium hydroxide (NaOH) (Sigma Aldrich), p-Toluenesulfonyl chloride (TsCl) (DAEJUNG), Lithium Chloride Anhydrous (LiCl) (DAEJUNG), N,N-Dimethyl acetamide (DMAc) (Merck), Triethylamine (TEA), Hydrazinium hydroxide (Merck), Diethylamine (DEA) (DAEJUNG), Copper Sulphate (Sigma Aldrich), Sodium borohydride ($NaBH_4$) (Sigma Aldrich), Acetone (Merck), N,N-Dimethyl formamide (DMF), Chloroform (Merck), Ethanol (Merck) and Deionized water (DI) (Sigma Aldrich) were procured from commercial sources as mentioned. All chemicals used for the synthesis and preparation of desired catalysts and composites were of high purity and no further purification was needed.

2.1 Preparation of Oxidized Cellulose (OC)

Oxidized cellulose (OC) was synthesized by using acidic mixture and $NaNO_2$ as oxidizing agent. Mixture of Nitric acid and phosphoric acid were taken in 4:1 (v/v). To 70 mL solution of the acidic mixture, 5.0g of MCC and 1.0g of $NaNO_2$ was added simultaneously. An instantaneous creation of reddish-brown fumes occurred. The reaction was continued for 48hrs at room temperature with occasional stirring. After 48hrs the mixture seemed greenish in color. An excess of distilled water was added to the reaction mixture. The green color disappeared, and white fluffy solid was acquired. This mixture was filtered and washed several times with distilled water till the pH of filtrate become 4. Solid obtained was finally washed with acetone and dried [36]. (Figure 2)

2.2 Tosylation of Microcrystalline Cellulose

Tosylation of cellulose has been performed according to previously reported method [37]. Briefly, MCC (5.0 g, 30.8 mmol of anhydroglucose unit (AGU)) in 500 mL round bottom flask was kept in vacuum oven for drying at 70 °C, 120 mL of DMAc was added to it, and stirred at 120-130 °C for two hrs. It was then cooled to 100 ℃ and 10 g anhydrous LiCl in 25 mL of DMAc were added under stirring. The stirring was sustained overnight until complete dissolution of MCC. A transparent gel like solution formed which indicates complete dissolution.

In second step a mixture of TEA (18.6ml, 185mmol, 6 mol/AGU) in 10 mL DMAc was added to the gel like solution of MCC under energetic stirring at room temperature (RT), the stirring was sustained for another 30 min, followed by the drop wise addition of p-toulenesulfonyl chloride (35.3 g, 184.8 mmol, 6 mol/AGU) (dissolved in 25 mL of DMA) over a period of 30 min at 3-8 °C. The stirring was continued for another 24 hrs at RT, then the mixture was poured slowly in 1L of ethanol. Precipitation occurs, the precipitate was filtered off, and washed carefully with approximately 1L of distilled water. Precipitates were further washed with ethanol (250 mL) for three times to remove unreacted TsCl. The resulted TsMCC was kept in an oven at 50 °C for 48 hrs for drying. (Figure 2)

2.3 Synthesis of 6-deoxycellulose amine derivatives

6-deoxycellulose amine derivatives of MCC were synthesized by replacing tosyl group with hydrazine and N,N-diethylamine by employing a method similar to previously reported method [38]. 2 g of TsMCC was mixed with 20 mL of DMF in 100 mL round bottom flask at room temperature. The reaction mixture was allowed to react under stirring until the complete dissolution. Then addition of 10 mL hydrazine hydrate was done under stirring, the stirring was continued for another 2 hrs at RT and then the reaction mixture was refluxed at 80 °C for 24 hrs. Orange color solution containing 6-Deoxycellulose hydrazide (MCC-Hyd) was obtained. This mixture was allowed to cool and then poured slowly into 250 mL of ethanol; formation of white precipitates occurred. This was then filtered and washed with ethanol thrice and dried at 50 °C under vacuum for 24 hrs.

Similar procedure was followed for the synthesis of 6-deoxycellulose(N,N-diethyl)amine (MCC-DEM) where N,N-Diethylamine was added in place of Hydrazine. (Figure 2)

2.4 Preparation of MCC and modified MCC films

Composite films of cellulose and modified cellulose were prepared by mechanical mixing. **Styrene-isoprene block copolymers (SIS)** polymer was used as a binding agent to strengthen the films. 0.1 g SIS was dissolved in 20 mL of chloroform under continuous stirring at room temperature. 1 g MCC or its derivatives was dispersed in this mixture, stirring was continued for 1 hr, after the complete dispersion the mixture was poured into petri dishes and left overnight for evaporation. Dried films were then peeled off and used further.

2.5 Preparation of copper nanoparticles

Copper nanoparticles were synthesized inside the layers of polymer films by uptake of Cu(II) ions followed by their reduction. Prepared films were dipped in 100 mL of 1M $CuSO_4.7H_2O$ solution for adsorption of Cu(II) ions. Films were left in copper sulphate solution of 24hrs for saturation of adsorption sites. After adsorption films were washed with D.I water and then kept in 50 mL of 0.5M $NaBH_4$ solution to reduce Cu(II) ions to Cu^0 nanoparticles. After that Cu^0 embedded polymeric films were washed gently with deionized water and used freshly.

2.6 Catalytic Reduction Studies

The catalytic reduction studies were performed for 4-nitrophenol (4-NP) and various azo dyes (Congo Red (CR), Methylene Blue (MB), and Methyl orange (MO)) reductions using sodium borohydride. Quartz cuvette cell was used as reaction container. Solutions of 4-NP, dyes and sodium borohydride were prepared in D.I water with concentrations of 0.5 mM, 0.08 mM and 0.5 M respectively. 3 mL of 0.08 mM 4-Nitrophenol was taken in a cuvette cell to which 0.5 mL of 0.5 M freshly prepared $NaBH_4$ solution was added and its spectra on UV visible spectrophotometer was recorded. After that, Cu°-MCC strips were placed in this cuvette cell in such a position that UV light can easily pass through it. Reduction reaction was started as soon as the catalyst strips were placed in reaction vessel (cuvette) and absorption spectra was continuously recorded.

The variations in absorbance value at 400 nm for 4-NP was plotted. For the reduction of other dyes (CR, MB, MO) same procedure was employed. Moreover, the degradation rate was also compared for each sample (catalyst) in the manner of percentage efficiency, which was calculated using following equation.

$$\% \, Efficiency = \left\{\left(\frac{A_0 - A_t}{A_0}\right)\right\}$$

Where, A_0 is initial absorbance while A_t is absorbance at time t.

2.7 Characterization

Scanning electron microscope (SEM, JEOL JSM-7600f, Japan) was performed to find the morphology and presence of Cu-Nps over the surface of MCC and derived MCC films. Elemental analysis of modified MCC derivatives was conducted by elemental analyzer (CKIC 5E-CHNS-2200 and CKIC5E-IRS II ultimate analyzer). The presence of Cu-Nps were further analyzed by XRD Using JEOL-JDX-II, X-ray diffractometer. Bruker attenuated total reflectance Fourier transform infrared (ATR FT-IR) spectrophotometer (Bruker platinum ATR model Alpha spectrophotometer, Germany) in the range of 400cm^{-1}-4000cm^{-1} was used to perform FT-IR analysis. ^{1}HNMR spectra were recorded for all samples at room temperature in deuterated dimethyl sulfoxide (DMSO-d6) on a 400 MHz Bruker AV400 spectrometer (Bruker corporation MA, USA) with 64 scans for concentration of 20 mg/mL^{-1}. The reduction in dyes concentration with the passage of time was evaluated via (Thermo-scientific evolution-300) UV/VIS spectrophotometer.

3. Results And Discussion

3.1 FTIR Analysis

The FT-IR spectra of MCC and prepared derivatives is shown in Figure 3. Examination of MCC showed a broad absorption band at 3325 cm^{-1} for –OH stretching. –OH, bending was observed at 1372 cm^{-1} while –CH bending was at 1236 cm^{-1} and epoxy stretching at 1024 cm^{-1} corresponds to glycosidic linkage in the structure of cellulose. Peaks allocated were well assigned and extensively described in previous literature [22, 39, 40].(Fig. 3a). Spectrum of oxidized cellulose showed a strong absorption band at 1728 cm^{-1} corresponds to the presence of carbonyl stretching, confirms the presence of acidic group (oxidation) (Fig. 3b). FT-IR analysis of tosylated cellulose (Fig. 3c) showed additional band of $–SO_2$ asymmetric stretch at 1355 cm^{-1}. A band of $–SO_2$ symmetric stretch is observed at 1175 cm^{-1}. At 815 cm^{-1} the band observed corresponds to –S-O-C stretching vibrations proving successful substitution[37, 41]. After the reaction with hydrazine hydrate in MCC-Hyd, the additional bands appeared at 3384 cm^{-1} and 3240 cm^{-1} for N-H Stretch and at 1337 cm^{-1} corresponds to C-N stretching vibration in the spectrum justifies that surface is functionalized with hydrazine hydrate (Fig. 3d). Following absorption bands has been observed for MCC-DEM, a strong absorption band at 3384 cm^{-1} for –OH stretch, -CH stretch at 2976 cm^{-1}, 1373 cm^{-1}, and 1464 cm^{-1} for $–CH_2$ and $–CH_3$ bending, respectively. The strong band at 1361 cm^{-1} confirms the presence of –C-N stretch (Fig. 3e).

3.2 ^{1}HNMR Analysis

^{1}H-NMR spectroscopy was used to obtain the information about the local environment of the proton in the MCC and its derivatives shown in Figure 4. Pristine MCC peaks appear between 3-5.5 ppm [42]. In ^{1}HNMR of OC chemical shift values appeared downfield around 12.58 ppm is justified by the close vicinity of highly electronegative oxygen atom. In ^{1}HNMR of Ts-MCC benzene ring proton appeared at 7.75 CH, 7.35 CH ppm while methyl group CH_3 appears at 2.42 ppm [38, 43]. For MCC-Hyd single NH appeared as a sharp signal at 6.2 ppm while NH_2 protons expected to appear at 3.23 ppm was masked under MCC backbone peaks. In case of MCC-DEM there was no peak for NH observed, suggesting the bonding occurred between Nitrogen and methylene of MCC. DEA CH_2 multiplet and CH_3 triplet appeared at 2.59 and 1.15 ppm, respectively [38]. ^{1}H-NMR of MCC derivatives is in good agreement with the relevant FTIR results.

3.3 Elemental Analysis

Elemental analysis (CHNS analysis) was useful in obtaining the degree of substitution by finding out the percentage of the elements found in the sample. Sulfur analysis of tosylated cellulose (Ts-MCC) was used to find degree of tosylation, which was found to be 42 % based on Sulfur analysis. Nitrogen analysis was carried out for the MCC-Hyd and MCC-DEM. Degree of amination was found to be 0.40 to 0.43, suggesting that the maximum number of tosyl group has been removed. Elemental analysis data in Table 1 proved that there is no chlorine moiety resulting from a side product. No polymer degradation resulted in the synthesis reaction. Yield of the reactions was more than 80%. In all the derivatives, a trace amount of sulfur of 0.5% and 1.01% for MCC-Hyd and MCC-DEM was found, respectively. Complete elimination of Tosyl group was not possible due to the polymeric structure of the Cellulose, but Nitrogen content of 12.26% and 5.43% was found in case of MCC-Hyd, MCC-DEM respectively. Results revealed that upon substitution with amino groups a considerable amount of nitrogen content was observed which indicates the successful preparation of both the derivatives.

Table 1. Elemental (CHNS) analysis of synthesized cellulose derivatives

Sr. No.	Sample Code	Carbon % (Found)	Hydrogen % (Found)	Nitrogen % (Found)	Sulfur % (Found)
1.	MCC-Hyd	38.93	6.53	12.26	-
2.	MCC-DEM	47.44	6.43	5.43	-
3.	Ts-MCC	31.34	4.16	-	4.49

3.4 XRD Analysis

The XRD spectra of MCC, OC, MCC-Hyd, and MCC-DEM are shown in Figure 5. In order to investigate the effect of cellulose modification by the amine groups, the crystal structure of the cellulose and its aminated Cellulose derivatives were analyzed with wide angle powder X-ray diffractogram shown in Figure 5(a, b). qualitative evaluation of all the spectra showed characteristic peaks of monolithic cellulose type 1 at 2θ values of 14.9°, 16.4°, 22.7°, and 34.6° with corresponding lattice planes of (11(-)0), (110), (200) and (004) respectively, as in other studies[16, 35, 44]. The cellulosic diffraction pattern altered as stated in previous studies [45] after the tosylation and modification with amine groups indicating that all the chemical modification dissolution of Cellulose [46] in LiCl/DMA mixture affected the lattice structure and altered the crystallinity of the cellulose as appeared from reasonable lowering of the peak intensity. Ts-MCC displayed a broad peak at 2θ = 20◦ (021) of amorphous
cellulose II [47, 48].

Figure 6 graph (a, b, c, and d) displays the XRD analysis of copper nanoparticles embedded films of MCC, OC, MCC-Hyd, and MCC-DEM respectively. All spectra show additional peaks at 2θ 43.2° (111), 50.3° (200) and 73.9° (220) (JCPDS no 89-2838) that are the distinctive diffraction peaks belongs to copper nanoparticles. Some additional peaks at 2θ 36.4°, 42.2°, 61.3° and 73.5° corresponding to JCPDS no 05-0667 were also observed in these spectra. These may occur due to the formation of copper oxide because copper is readily oxidized to CuO and Cu_2O. Modified cellulose derivatives (OC, MCC-Hyd, and MCC-DEM) showed low crystallinity [49] with characteristic near amorphous form [50] as illustrated in Figure 6 graph (b, c, and d). The decrease in crystallinity of derivatives from original microcrystalline cellulose during modification is due to the disturbance of inter and intramolecular chains of cellulose structure.

3.5 SEM Analysis

Figure 7 shows SEM images of films from pure MCC and its derivatives with and without Cu NPs. Pure MCC has homogeneous structure while the derivatives have an interconnected heterogeneous structure. In case of films having MCC and its derivatives embedded with the Cu NPs presence of small granules confirms that Cu NPs successfully templated in the MCC and its derivatives with the polymer support.

3.6 Degradation studies

Degradation experiments were carried out on 4NP, CR, MB, and MO dye. For this purpose, a stock solution of 0.5 mM for 4NP and 0.1 mM for dyes (CR, MB, and MO) was made which was further diluted up to 0.05Mm and 0.08Mm for 4NP and dyes, respectively. Degradation studies were carried out for all the prepared samples. For all catalysts $0.5cm^2 \times 1cm^2$ strips, 2.5 mL of aqueous solution of dyes and 0.5 mL of $NaBH_4$ solution was used[22, 51]. Reaction was carried out in quartz cuvette cell and spectra was recorded on spectrophotometer.

First bare MCC-DEM film was placed in UV cuvette containing 2.5 mL of aqueous solution of 4NP and 0.5 mL of $NaBH_4$ and its spectra was recorded every minute till half an hour. The typical peak of 4-NP absorbance appeared at λ_{max} 310 nm, which shifted to 400 nm by the addition of $NaBH_4$ solution, reason behind is

extended conjugation. Figure 8 (a) shows that no change in absorbance intensity at 400 nm was observed [22, 35]. Which shows the poor catalytic performance of bare MCC-DEM film towards the reduction of 4NP. The reduction of 4np in absence of suitable catalyst is difficult to achieve due to the high kinetic barrier between phenolate ions ($C_6H_4NO^{3-}$) and borate ions (BH^{4-}).

After that under similar conditions Cu^0 loaded strip was introduced to the cuvette containing reaction mixture. Change in color of 4NP was observed, it starts disappearing as soon as the Cu^0 strip was introduced. Fig. 8 (b) shows that absorbance intensity of peak at 400nm progressively decreases and completely disappeared after 19mints, show excellent catalytic reduction of 4NP by Cu^0 loaded MCC-DEM film as compared to previous studies [35]. Fig. 8(c) illustrate the activity of all the prepared samples in the presence of ZVC NPs against degradation of 4-NP with the passage of time in terms of $\%C_t / C_o$. It is clear from figure that all samples incorporated with Cu^0 show excellent efficiency, but highest efficiency was observed with Cu-OC in minimum time. Fig. 8(d) shows percentage degradation efficiency of all prepared Cu^0 loaded films against 4-NP degradation. All ZVC nps loaded films show excellent degradation efficiency, highest efficiency achieved for 4-NP was 99%. The natural log ($\ln C_t/C_0$) of the absorption peak at λ_{max} 400nm Vs time indicating a large linear portion. This validates that reaction proceeds with pseudo first order kinetics. The rates of reaction were 1.30×10^{-1}, 1.75×10^{-1}, 2.17×10^{-1} and 2.53×10^{-1} min^{-1} for Cu-MCC, Cu-MCC-DEM, Cu-MCC-Hyd, and Cu-OC respectively.

Figure 9 graph (b) depict gradual decrease in absorbance at wavelength 498 nm after every minute. Cu^0-MCC-DEM takes 10 minutes to degrade CR to 88.8%. Fig. 9(c) illustrate the activity of all the prepared samples against degradation of CR with the passage of time in terms of C_t / C_o. It is clear from figure that all samples showed excellent efficiency, but highest efficiency was observed with Cu-MCC-Hyd in minimum time of 8 min. Fig. 9(d) shows percentage degradation efficiency of all prepared films against CR degradation. All ZVC nps loaded films show excellent degradation efficiency, highest efficiency achieved for CR degradation was 94.2 % with MCC-Hyd film in the presence of ZVC nps. The graph obtained as a result of $\ln C_t/C_0$ Vs time suggest that degradation reaction of CR in the presence of ZVC nps proceeds with pseudo first order kinetics. The rates of reactions were 2.37×10^{-1}, 2.53×10^{-1}, 2.78×10^{-1} and 1.81×10^{-1} min^{-1} for Cu-MCC, Cu-MCC-DEM, Cu-MCC-Hyd, and Cu-OC respectively.

Figure 10 shows degradation spectra of methylene blue with amino modified cellulose MCC-DEM. Cu^0-MCC-DEM (Fig. 10b) takes 13 min to degrade MB to 91%. CR takes minimum time of 9min and maximum of 13min to show its catalytic activity (Fig. 10c). Highest degradation efficiency of 94.8% has been observed with Cu^o-MCC-Hyd films in 11min (Fig. 10d). Reaction kinetic was found to be pseudo first order (fig. 10e). Reaction rates obtained for Cu-MCC, Cu-MCC-DEM, Cu-MCC-Hyd and Cu-OC were 1.25×10^{-1}, 1.56×10^{-1}, 2.68×10^{-1} and 3.36×10^{-1} min^{-1} respectively.

Similarly, Figure 11 shows degradation spectra of methyl orange with MCC-DEM with and without nanoparticles. No change in absorbance occurred in the absence of zero valent nanoparticles (Fig. 11a) while decrease in absorbance at λ_{max} 464nm with the passage of time was observed with Cu^0 loaded MCC-DEM film (Fig. 11b). Cu^o-MCC-DEM Shows catalytic activity in 10min (Fig. 11c). Fig. 11d shows degradation of all

prepared films incorporated with ZVC in terms of percentage efficiency. Highest efficiency of 89.9% has been observed for MO, which is more than previously reported study[34]. Linearity of graph ln C_t/C_0 Vs. time depict pseudo-first order kinetics and rate of reactions were 1.95×10^{-1}, 1.81×10^{-1}, 1.89×10^{-1} and 2.2×10^{-1} min^{-1} for Cu-MCC, Cu-MCC-DEM, Cu-MCC-Hyd and Cu-OC respectively.

Figure 12 illustrates the percentage efficiencies of all the samples for all four dyes. Graphs shows that Modified cellulose showed excellent degradation efficiency for all dyes. Oxidized cellulose showed highest efficiency in almost all cases. While amino modified derivatives also exhibit more than 85% efficiency in all cases. The percent degradation of all the dyes and required time for it are summarized in Table 2 as well.

Table 2. Summary of Degradation Results with different Dyes.

Sample	4-NP		CR		MB		MO	
	% Degradation	Time (min)	% Degradation	Time (min)	% Degradation	Time (min)	% Degradation	Time (min)
MCC	88	19	77	11	85.4	10	77.9	12
OC	99	8	85	10	93.4	9	91.3	10
MCC-Hyd	91	11	94.2	8	94.8	11	89.9	11
MCC-DEM	89.6	12	88.8	10	91	13	89.5	10

4. Conclusion

Here in this study, carboxylic acid and amino functionalized cellulose derivatives *viz.* oxidized cellulose (OC), 6-Deoxycellulosehydrazide (MCC-Hyd) and 6-deoxycellulose(N,N-diethyl) amine (MCC-DEM) were successfully synthesized. Cellulose and its synthesized derivatives were employed for uptake of copper ions from aqueous solution. Films of cellulose and modified cellulose was successfully prepared and used as support materials for zero valent copper nanoparticles. Chemical reduction method was used for the synthesis of Zero valent copper nanoparticles. OC, MCC-Hyd and MCC-DEM showed excellent degradation efficiency in the presence of Cu^0 nanoparticles. In most the of cases amino modified cellulose showed highest degradation efficiency probably due to larger uptake of Cu(II) ions because of the presence of more adsorption sites (NH_2 groups) which fix the metal ion in polymer matrix by dipole-ion interactions and electrostatic forces.

Declarations

Acknowledgement

The authors thank School of Natural Sciences (SNS), National University of Sciences and Technology (NUST), for providing all facilities for the completion of the project.

Funding

This research received no external funding.

Compliance with Ethical Standards

1. The authors declare to have no conflicts of interest.
2. The research do not involve any Human or Animal and informed consent is not applicable in this case

References

1. Ali, N., et al., *Chitosan-coated cotton cloth supported copper nanoparticles for toxic dye reduction.* International journal of biological macromolecules, 2018. **111**: p. 832-838.
2. Haines, A., et al., *Climate change and human health: impacts, vulnerability and public health.* Public health, 2006. **120**(7): p. 585-596.
3. Raaschou-Nielsen, O., et al., *Air pollution and lung cancer incidence in 17 European cohorts: prospective analyses from the European Study of Cohorts for Air Pollution Effects (ESCAPE).* The lancet oncology, 2013. **14**(9): p. 813-822.
4. Sha, Y., et al., *Rapid degradation of azo dye methyl orange using hollow cobalt nanoparticles.* Chemosphere, 2016. **144**: p. 1530-1535.
5. Youssef, N.A., et al., *Degradation of methyl orange using Fenton catalytic reaction.* Egyptian Journal of Petroleum, 2016. **25**(3): p. 317-321.
6. Spadaro, J.T., L. Isabelle, and V. Renganathan, *Hydroxyl radical mediated degradation of azo dyes: evidence for benzene generation.* Environmental science & technology, 1994. **28**(7): p. 1389-1393.
7. Robinson, T., et al., *Remediation of dyes in textile effluent: a critical review on current treatment technologies with a proposed alternative.* Bioresource technology, 2001. **77**(3): p. 247-255.
8. Amoozegar, M.A., et al., *Azo dye decolorization by halophilic and halotolerant microorganisms.* Annals of Microbiology, 2011. **61**(2): p. 217-230.
9. Parshetti, G., et al., *Decolorization and detoxification of sulfonated azo dye methyl orange by Kocuria rosea MTCC 1532.* Journal of Hazardous Materials, 2010. **176**(1-3): p. 503-509.
10. Min, M., et al., *Micro-nano structure poly (ether sulfones)/poly (ethyleneimine) nanofibrous affinity membranes for adsorption of anionic dyes and heavy metal ions in aqueous solution.* Chemical engineering journal, 2012. **197**: p. 88-100.
11. Chen, Q., et al., *Precipitation of heavy metals from wastewater using simulated flue gas: sequent additions of fly ash, lime and carbon dioxide.* Water research, 2009. **43**(10): p. 2605-2614.
12. Razali, M., et al., *Sustainable wastewater treatment and recycling in membrane manufacturing.* Green Chemistry, 2015. **17**(12): p. 5196-5205.
13. Teh, C.Y., et al., *Recent advancement of coagulation–flocculation and its application in wastewater treatment.* Industrial & Engineering Chemistry Research, 2016. **55**(16): p. 4363-4389.

14. Pal, S., et al., *Modified guar gum/SiO 2: development and application of a novel hybrid nanocomposite as a flocculant for the treatment of wastewater.* Environmental Science: Water Research & Technology, 2015. **1**(1): p. 84-95.
15. Da□browski, A., et al., *Selective removal of the heavy metal ions from waters and industrial wastewaters by ion-exchange method.* Chemosphere, 2004. **56**(2): p. 91-106.
16. Ismail, M., et al., *Green synthesis of zerovalent copper nanoparticles for efficient reduction of toxic azo dyes congo red and methyl orange.* Green processing and synthesis, 2019. **8**(1): p. 135-143.
17. Wang, J. and H. Gu, *Novel metal nanomaterials and their catalytic applications.* Molecules, 2015. **20**(9): p. 17070-17092.
18. Yang, J., et al., *Nickel nanoparticle–chitosan-reduced graphene oxide-modified screen-printed electrodes for enzyme-free glucose sensing in portable microfluidic devices.* Biosensors and Bioelectronics, 2013. **47**: p. 530-538.
19. Khan, A., et al., *A chemical reduction approach to the synthesis of copper nanoparticles.* International Nano Letters, 2016. **6**(1): p. 21-26.
20. Wang, P., et al., *Application of Au based nanomaterials in analytical science.* Nano Today, 2017. **12**: p. 64-97.
21. Kamal, T., S.B. Khan, and A.M. Asiri, *Synthesis of zero-valent Cu nanoparticles in the chitosan coating layer on cellulose microfibers: evaluation of azo dyes catalytic reduction.* Cellulose, 2016. **23**(3): p. 1911-1923.
22. Haider, S., et al., *Natural polymers supported copper nanoparticles for pollutants degradation.* Applied Surface Science, 2016. **387**: p. 1154-1161.
23. Zhou, Z., et al., *Cellulose nanocrystals as a novel support for CuO nanoparticles catalysts: facile synthesis and their application to 4-nitrophenol reduction.* RSC advances, 2013. **3**(48): p. 26066-26073.
24. Guo, Z., et al., *CuO nanoparticle filled vinyl-ester resin nanocomposites: Fabrication, characterization and property analysis.* Composites Science and Technology, 2007. **67**(10): p. 2036-2044.
25. Shokouhimehr, M., *Magnetically separable and sustainable nanostructured catalysts for heterogeneous reduction of nitroaromatics.* Catalysts, 2015. **5**(2): p. 534-560.
26. Bakhsh, E.M., et al., *Performance of cellulose acetate-ferric oxide nanocomposite supported metal catalysts toward the reduction of environmental pollutants.* International journal of biological macromolecules, 2018. **107**: p. 668-677.
27. Khan, S.A., et al., *A facile synthesis of CuAg nanoparticles on highly porous ZnO/carbon black-cellulose acetate sheets for nitroarene and azo dyes reduction/degradation.* International journal of biological macromolecules, 2019. **130**: p. 288-299.
28. Kamal, T., et al., *Dye adsorption and bactericidal properties of TiO2/chitosan coating layer.* Carbohydrate polymers, 2016. **148**: p. 153-160.
29. Wang, K.P., et al. *A novel gold nanoparticle/poly (AMPS-co-HEMA) composite hydrogel for selective catalysis*. in *Advanced Materials Research*. 2012. Trans Tech Publ.
30. Kamal, T., et al., *Synthesis and catalytic properties of silver nanoparticles supported on porous cellulose acetate sheets and wet-spun fibers.* Carbohydrate polymers, 2017. **157**: p. 294-302.

31. Jia, B., et al., *Preparation of copper nanoparticles coated cellulose films with antibacterial properties through one-step reduction.* ACS applied materials & interfaces, 2012. **4**(6): p. 2897-2902.
32. Yang, G., et al., *Antimicrobial activity of silver nanoparticle impregnated bacterial cellulose membrane: effect of fermentation carbon sources of bacterial cellulose.* Carbohydrate Polymers, 2012. **87**(1): p. 839-845.
33. Maneerung, T., S. Tokura, and R. Rujiravanit, *Impregnation of silver nanoparticles into bacterial cellulose for antimicrobial wound dressing.* Carbohydrate polymers, 2008. **72**(1): p. 43-51.
34. Li, P., et al., *Enhanced decolorization of methyl orange using zero-valent copper nanoparticles under assistance of hydrodynamic cavitation.* Ultrasonics sonochemistry, 2015. **22**: p. 132-138.
35. Ali, F., et al., *Chitosan coated cotton cloth supported zero-valent nanoparticles: simple but economically viable, efficient and easily retrievable catalysts.* Scientific reports, 2017. **7**(1): p. 1-16.
36. Kumar, V. and T. Yang, *HNO3/H3PO4–NaNO2 mediated oxidation of cellulose—preparation and characterization of bioabsorbable oxidized celluloses in high yields and with different levels of oxidation.* Carbohydrate Polymers, 2002. **48**(4): p. 403-412.
37. Rahn, K., et al., *Homogeneous synthesis of cellulose p-toluenesulfonates in N, N-dimethylacetamide/LiCl solvent system.* Die Angewandte Makromolekulare Chemie: Applied Macromolecular Chemistry and Physics, 1996. **238**(1): p. 143-163.
38. Nazir, F. and M. Iqbal, *Synthesis, Characterization and Cytotoxicity Studies of Aminated Microcrystalline Cellulose Derivatives against Melanoma and Breast Cancer Cell Lines.* Polymers, 2020. **12**(11): p. 2634.
39. Kenawy, I., et al., *Adsorption of Cu (II), Cd (II), Hg (II), Pb (II) and Zn (II) from aqueous single metal solutions by guanyl-modified cellulose.* International journal of biological macromolecules, 2018. **107**: p. 1538-1549.
40. Singha, A. and A. Guleria, *Chemical modification of cellulosic biopolymer and its use in removal of heavy metal ions from wastewater.* International Journal of Biological Macromolecules, 2014. **67**: p. 409-417.
41. Schmidt, S., T. Liebert, and T. Heinze, *Synthesis of soluble cellulose tosylates in an eco-friendly medium.* Green Chemistry, 2014. **16**(4): p. 1941-1946.
42. Guan, Y., et al., *Fabrication of biopolymer hydrogel containing Ag nanoparticles for antibacterial property.* Industrial & Engineering Chemistry Research, 2015. **54**(30): p. 7393-7400.
43. Heinze, T., et al., *Solvent-free synthesis of 6-deoxy-6-(ω-aminoalkyl) amino cellulose.* Journal of Applied Polymer Science, 2016. **133**(39).
44. Gericke, M., et al., *Studies on the tosylation of cellulose in mixtures of ionic liquids and a co-solvent.* Carbohydrate polymers, 2012. **89**(2): p. 526-536.
45. El-Sayed, N.S., et al., *New approach for immobilization of 3-aminopropyltrimethoxysilane and TiO2 nanoparticles into cellulose for BJ1 skin cells proliferation.* Carbohydrate polymers, 2018. **199**: p. 193-204.
46. Gupta, P., V. Uniyal, and S. Naithani, *Polymorphic transformation of cellulose I to cellulose II by alkali pretreatment and urea as an additive.* Carbohydrate polymers, 2013. **94**(2): p. 843-849.
47. El-Sayed, N.S., et al., *Synthesis and characterization of polyaniline/tosylcellulose stearate composites as promising semiconducting materials.* Synthetic Metals, 2018. **236**: p. 44-53.

48. Mittal, A., et al., *Effects of alkaline or liquid-ammonia treatment on crystalline cellulose: changes in crystalline structure and effects on enzymatic digestibility.* Biotechnology for biofuels, 2011. **4**(1): p. 1-16.
49. Park, S., et al., *Cellulose crystallinity index: measurement techniques and their impact on interpreting cellulase performance.* Biotechnology for biofuels, 2010. **3**(1): p. 1-10.
50. Demircan, D. and B. Zhang, *Facile synthesis of novel soluble cellulose-grafted hyperbranched polymers as potential natural antimicrobial materials.* Carbohydrate polymers, 2017. **157**: p. 1913-1921.
51. Konstantinou, I.K. and T.A. Albanis, *TiO2-assisted photocatalytic degradation of azo dyes in aqueous solution: kinetic and mechanistic investigations: a review.* Applied Catalysis B: Environmental, 2004. **49**(1): p. 1-14.

Figures

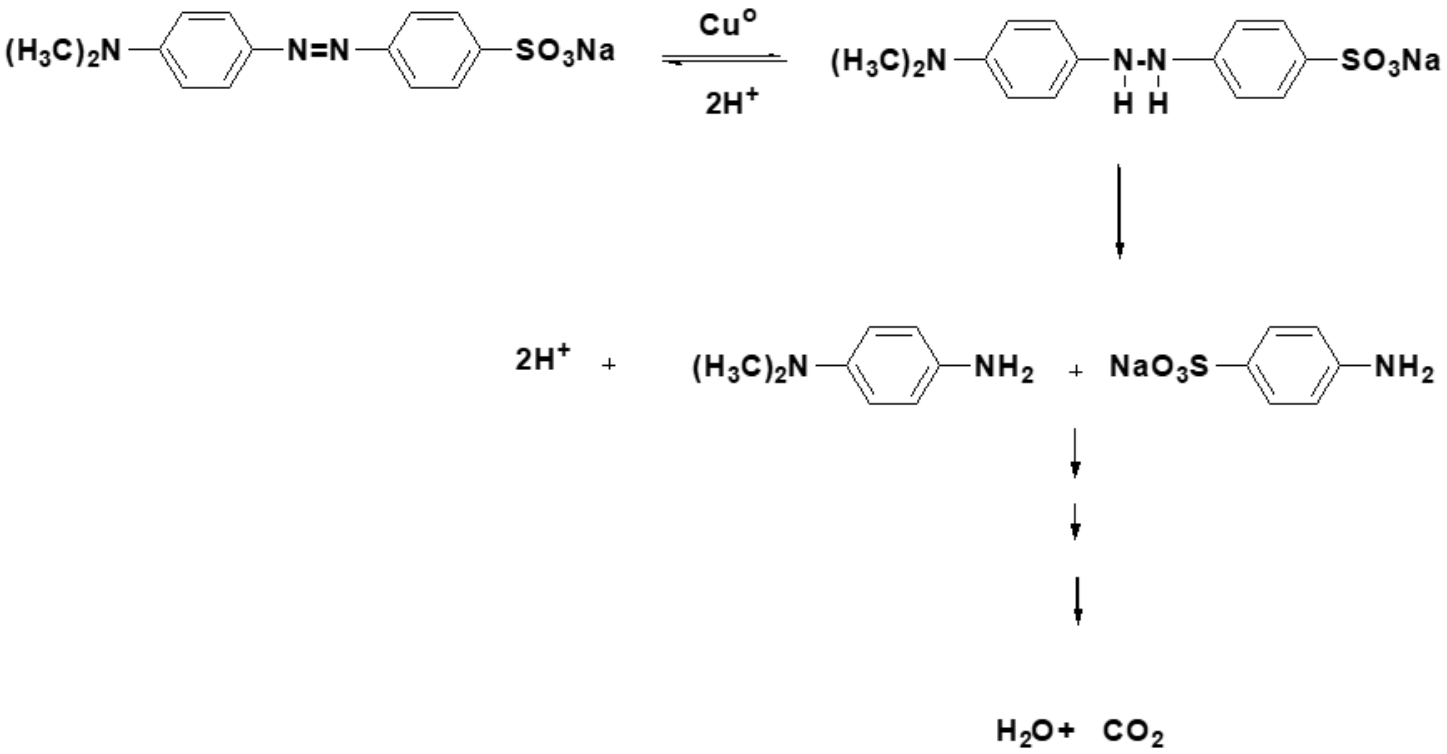

Figure 1

Proposed degradation mechanism.[34, 35]

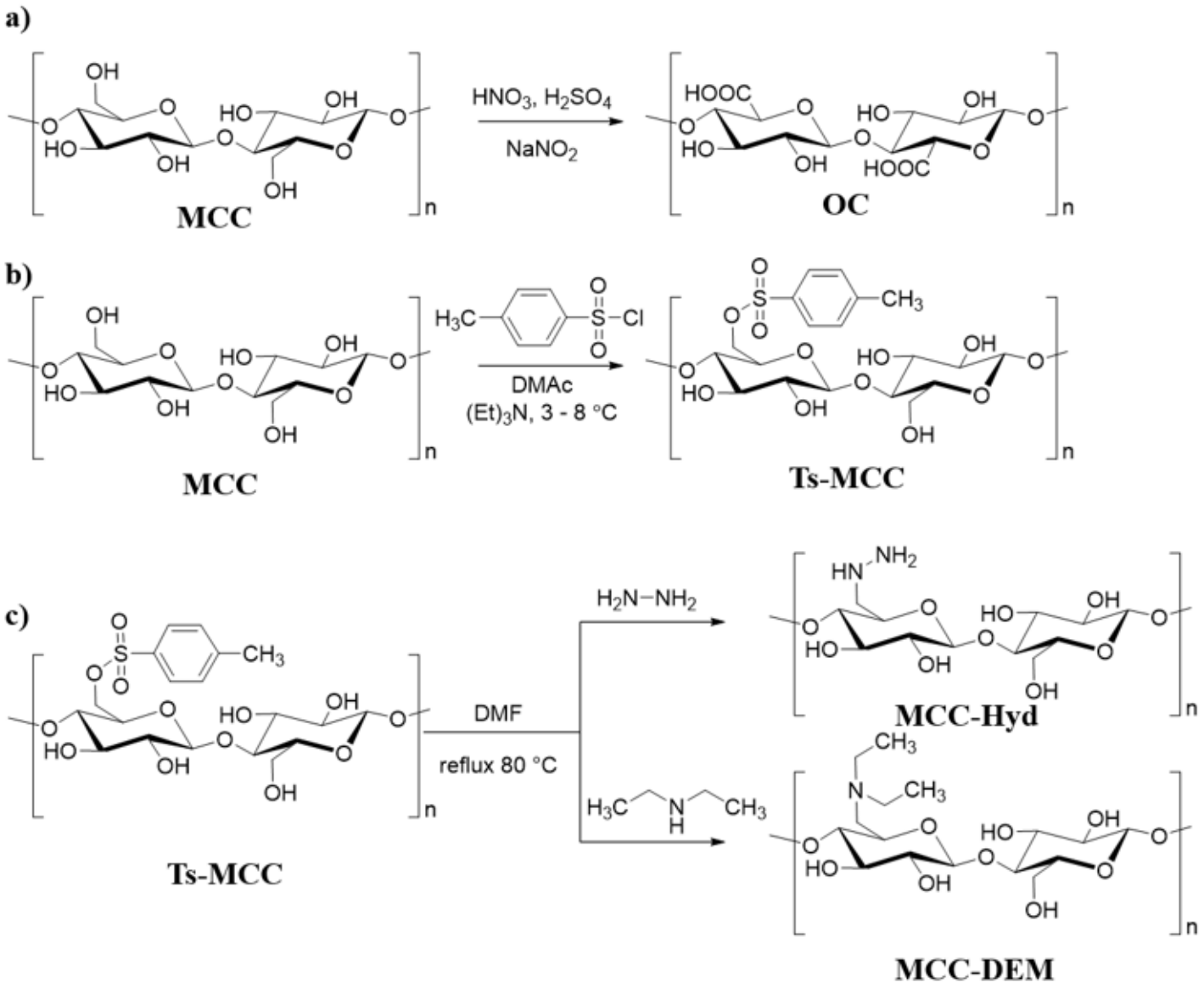

Figure 2

Scheme of Synthesis of Microcrystalline Cellulose (MCC) Derivatives (a) MCC oxidation (b) synthesis of Ts-MCC (c) Amine functionalization of TS-MCC to MCC-Hyd and MCC-DEM.

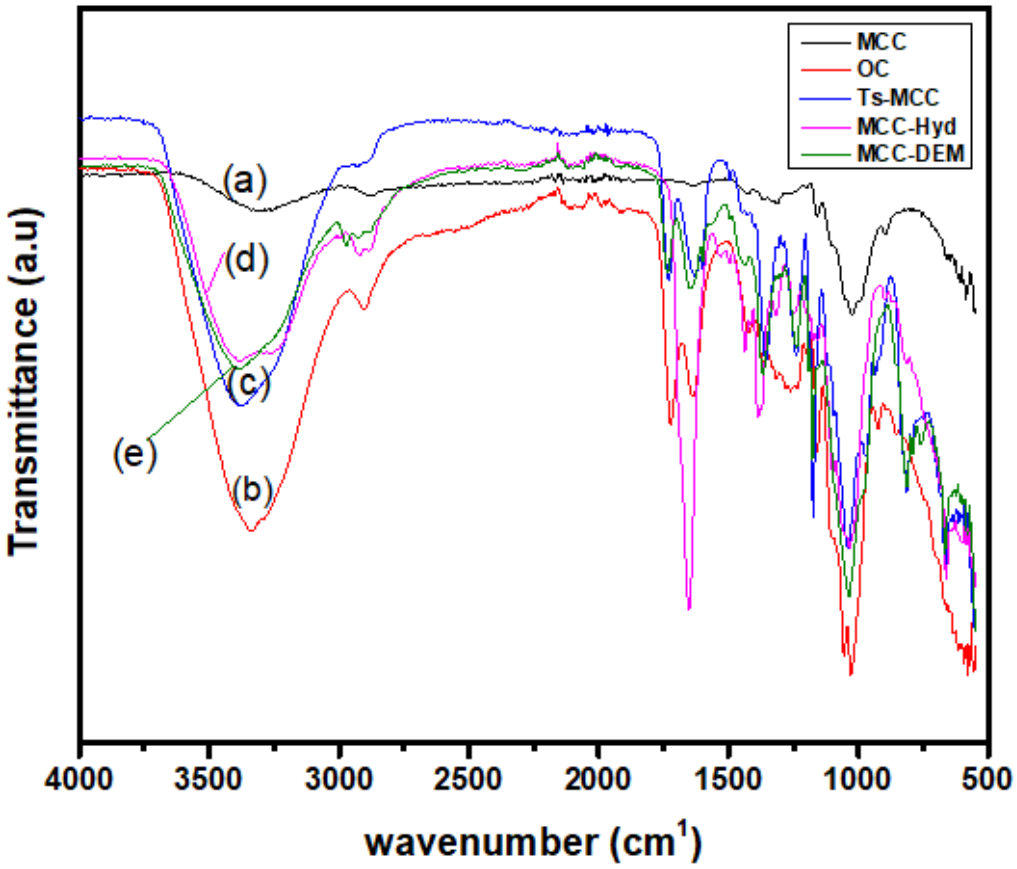

Figure 3

FTIR spectra of (a) pure MCC (b) OC (c) Ts-MCC (d) MCC-Hyd (e) MCC-DEM

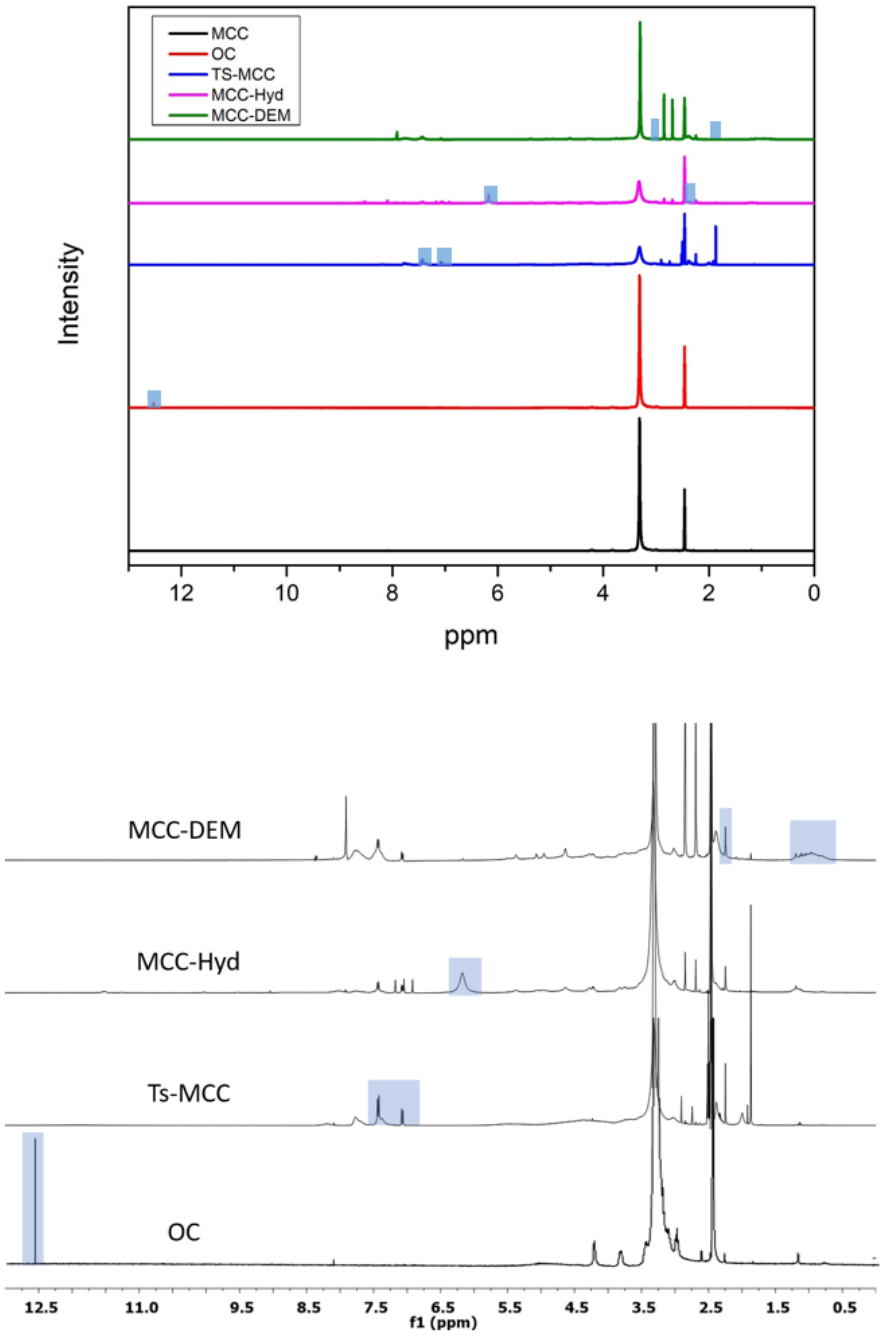

Figure 4

1HNMR spectra of OC, Ts-MCC, MCC-Hyd and MCC-DEM

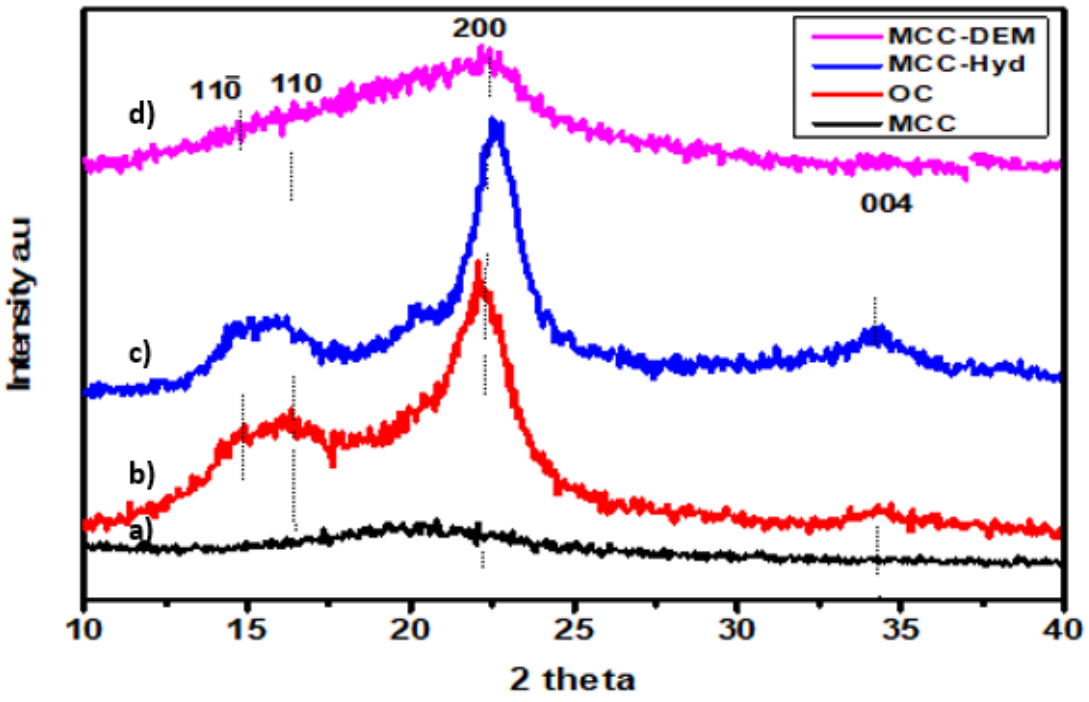

Figure 5

XRD pattern of pure MCC, OC, MCC-Hyd and MCC-DEM

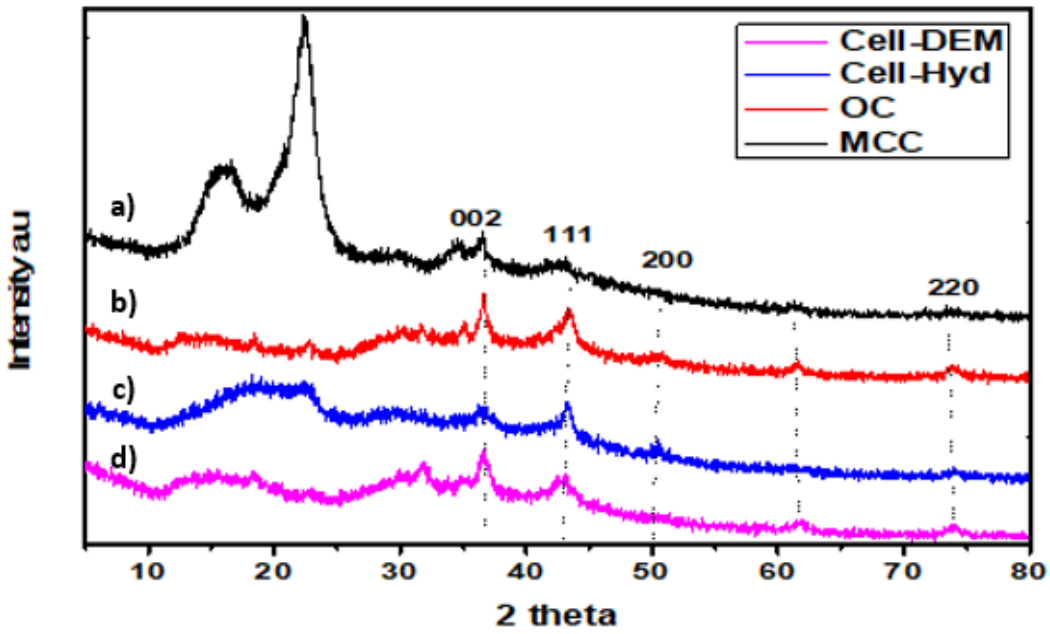

Figure 6

XRD Pattern of pure MCC, OC, MCC-Hyd, and MCC-DEM with embedded Cu nanoparticles

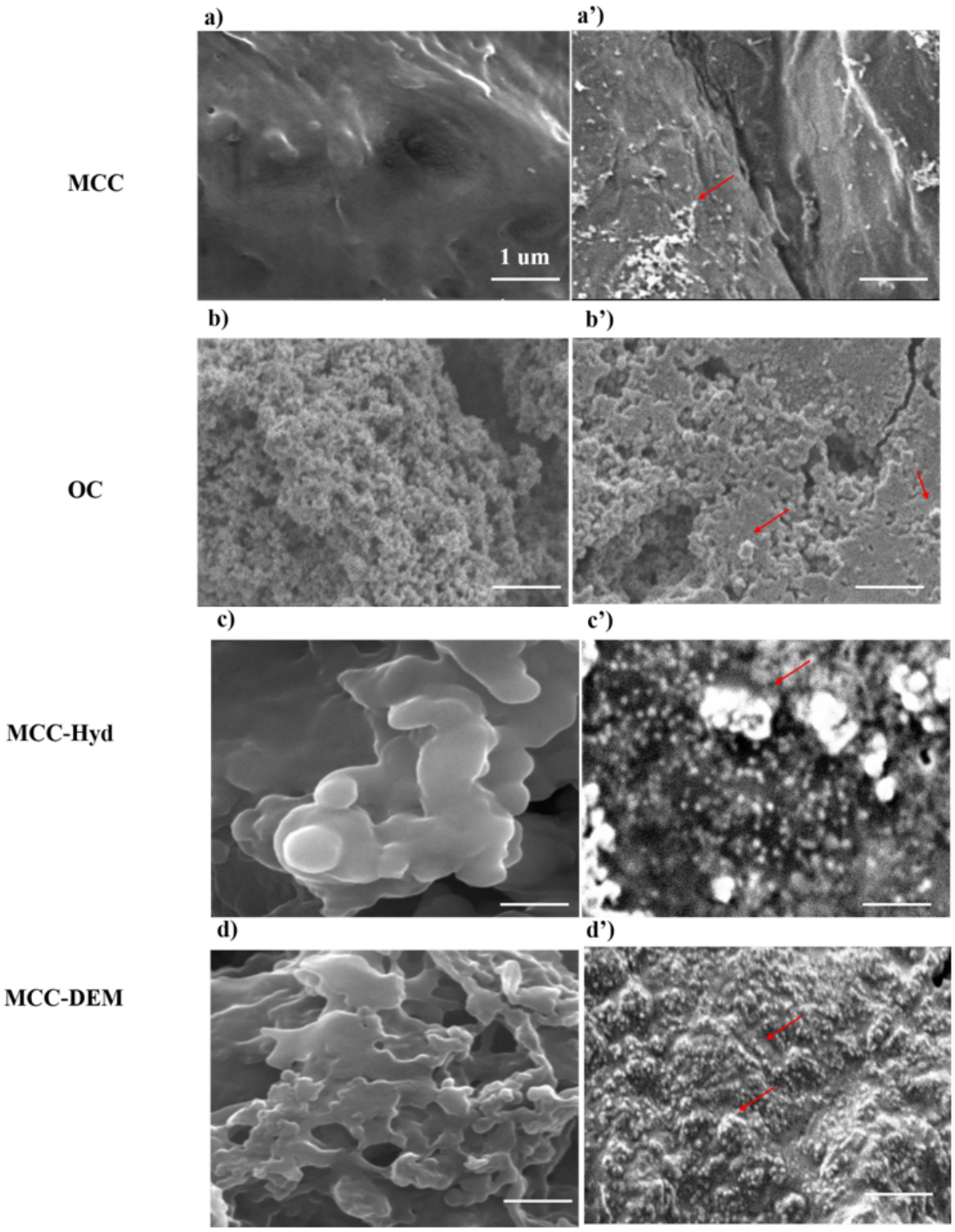

Figure 7

SEM Images of films of MCC and its derivatives a) MCC, b) OC, c) MCC-Hyd, d) MCC-DEM, a') MCC with Cu NPs (b') OC with Cu NPs (c') MCC-Hyd with Cu NPs (d') MCC-Hyd with Cu NPs. Red arrows show Cu NP s embedded in MCC and its derivatives in polymer films; Scale bar is 1um.

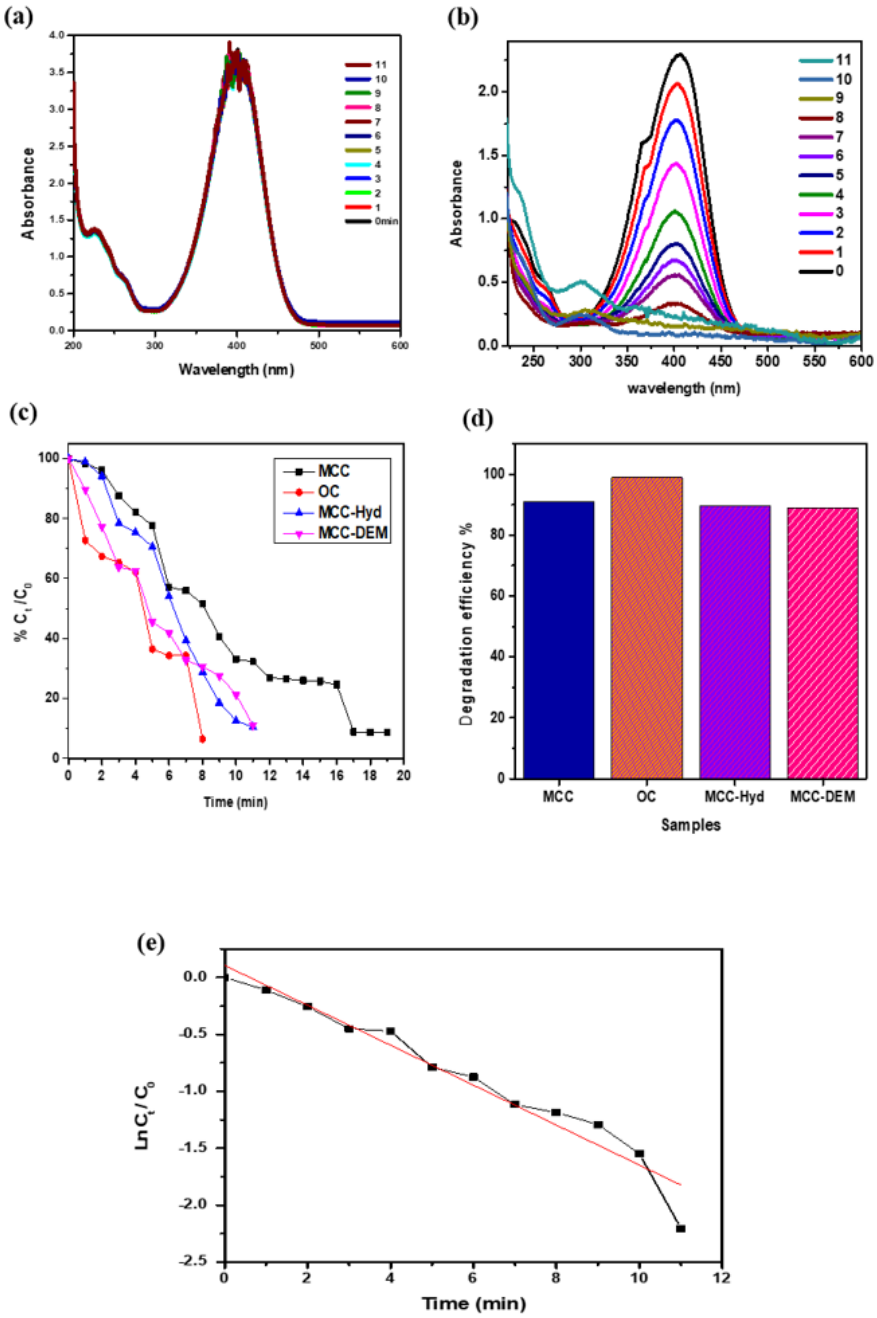

Figure 8

Absorption spectra of 4-NP at different interval of time. (a) Bare MCC-DEM film. (b) Cu-MCC-DEM film. (c) Activity of all prepared films incorporated with Cu0 Nps against 4-NP degradation (d) degradation efficiency of all films loaded with Cu0 Nps against 4-NP degradation. (e) Reaction kinetics obtained as a result of Ln Ct/C0. Experimental conditions: 0.08 Mm 2.5 mL of 4-NP, 0.5 mL NaBH4 0.5 M, 1 cm strip of each film.

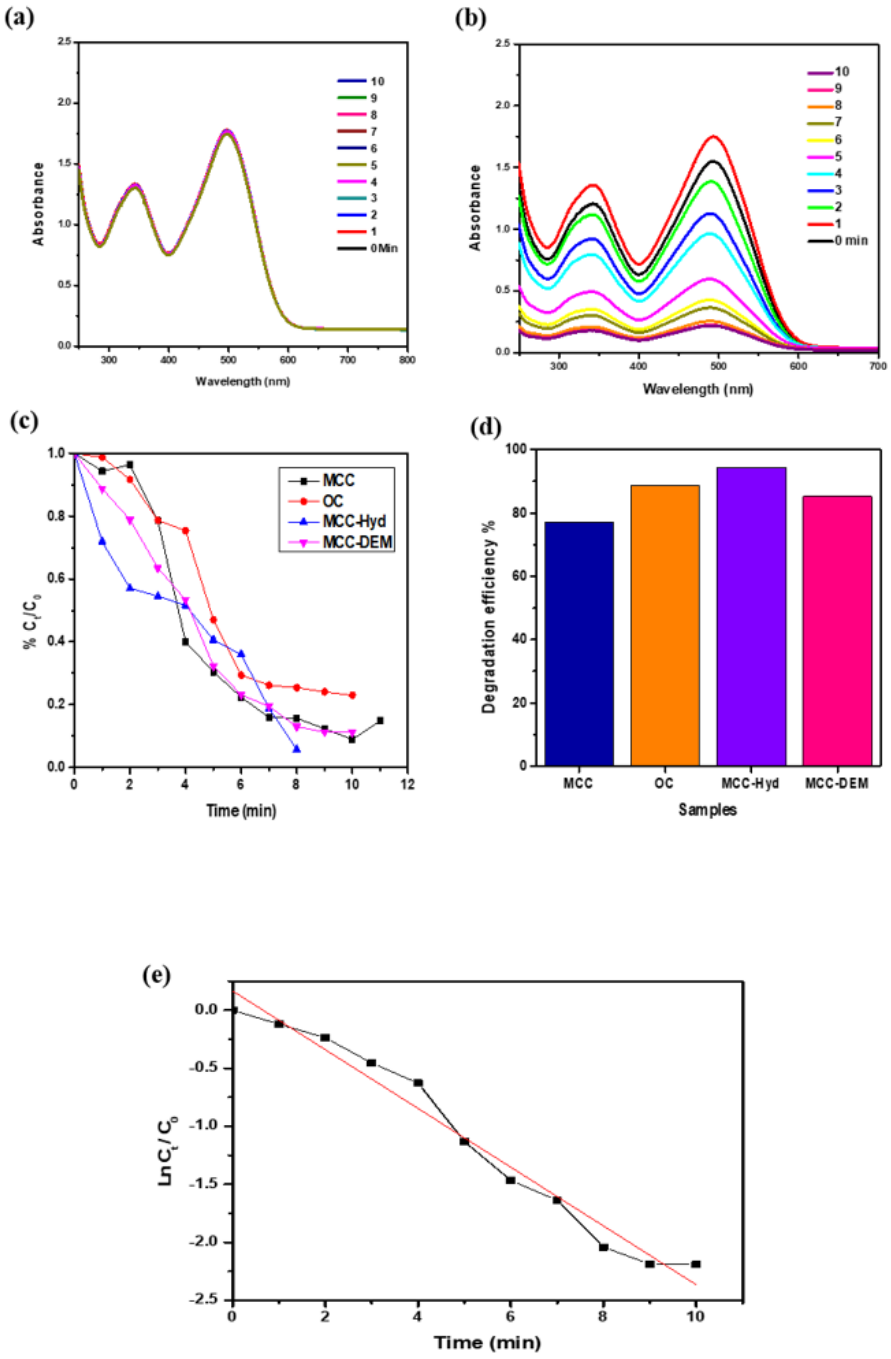

Figure 9

Absorption Spectra of Congo red aqueous solution at different interval of time. (a) Bare MCC-DEM film (b) Cu0-MCC-DEM film. (c) Activity of all prepared films incorporated with ZVC nps against CR degradation. (d) Degradation efficiency of all ZVC loaded films against CR degradation. (e) Reaction kinetics obtained as a result of Ln Ct/C0. Experimental conditions: 0.05 Mm 2.5 mL of 4-CR, 0.5 mL NaBH4 0.5 M, 1 cm strip of each film.

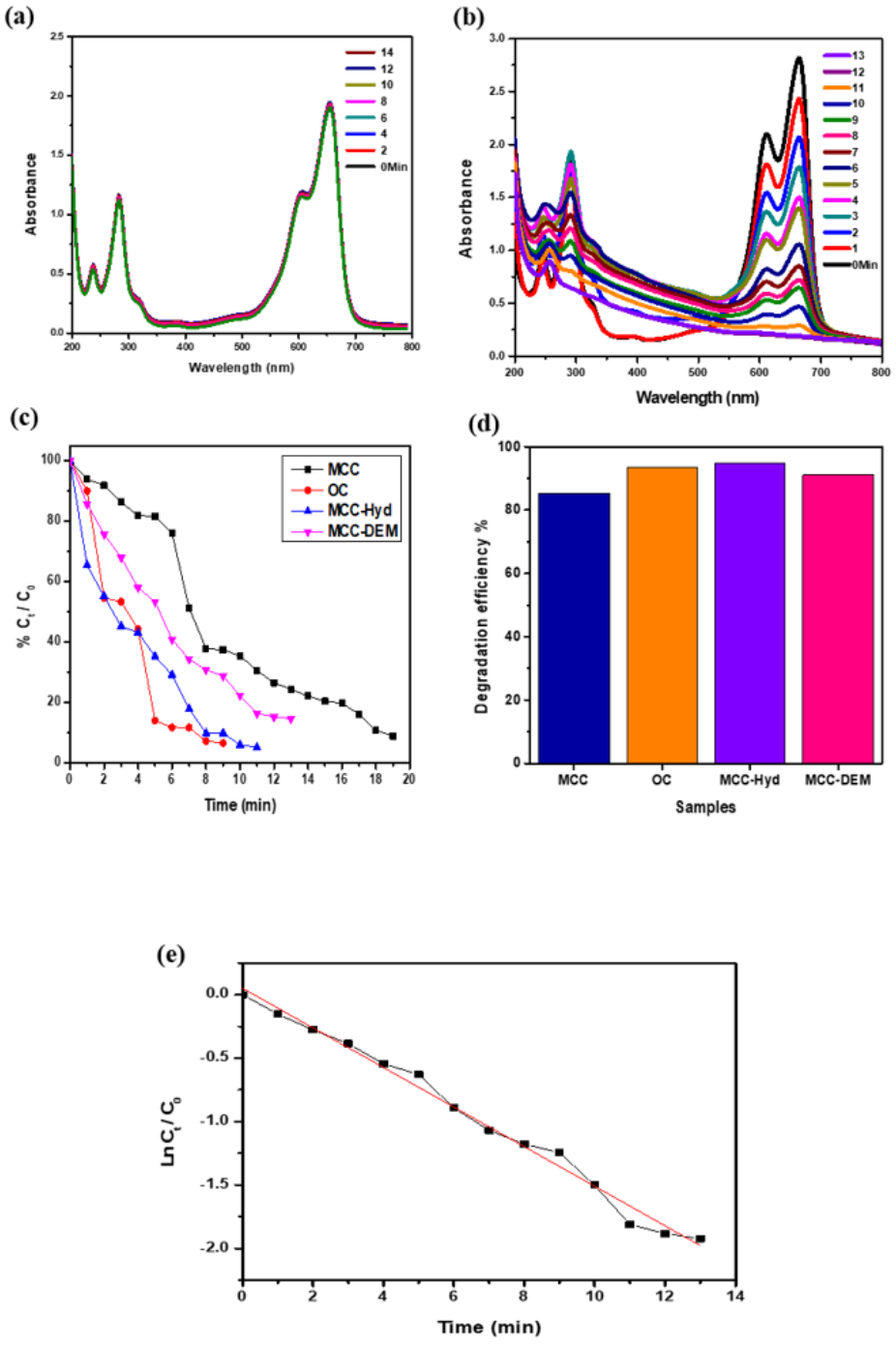

Figure 10

Absorbance Spectra of Methylene blue aqueous solution at different interval of time. (a) Bare MCC-DEM (b) Cu-MCC-DEM. (c) activity of all prepared films against MB degradation. (d) Degradation efficiency of all samples against MB degradation. (e) Reaction kinetics obtained as a result of Ln Ct/C0. Experimental conditions: 0.05 Mm 2.5 mL of 4-CR, 0.5 mL NaBH4 0.5 M, 1 cm strip of each film.

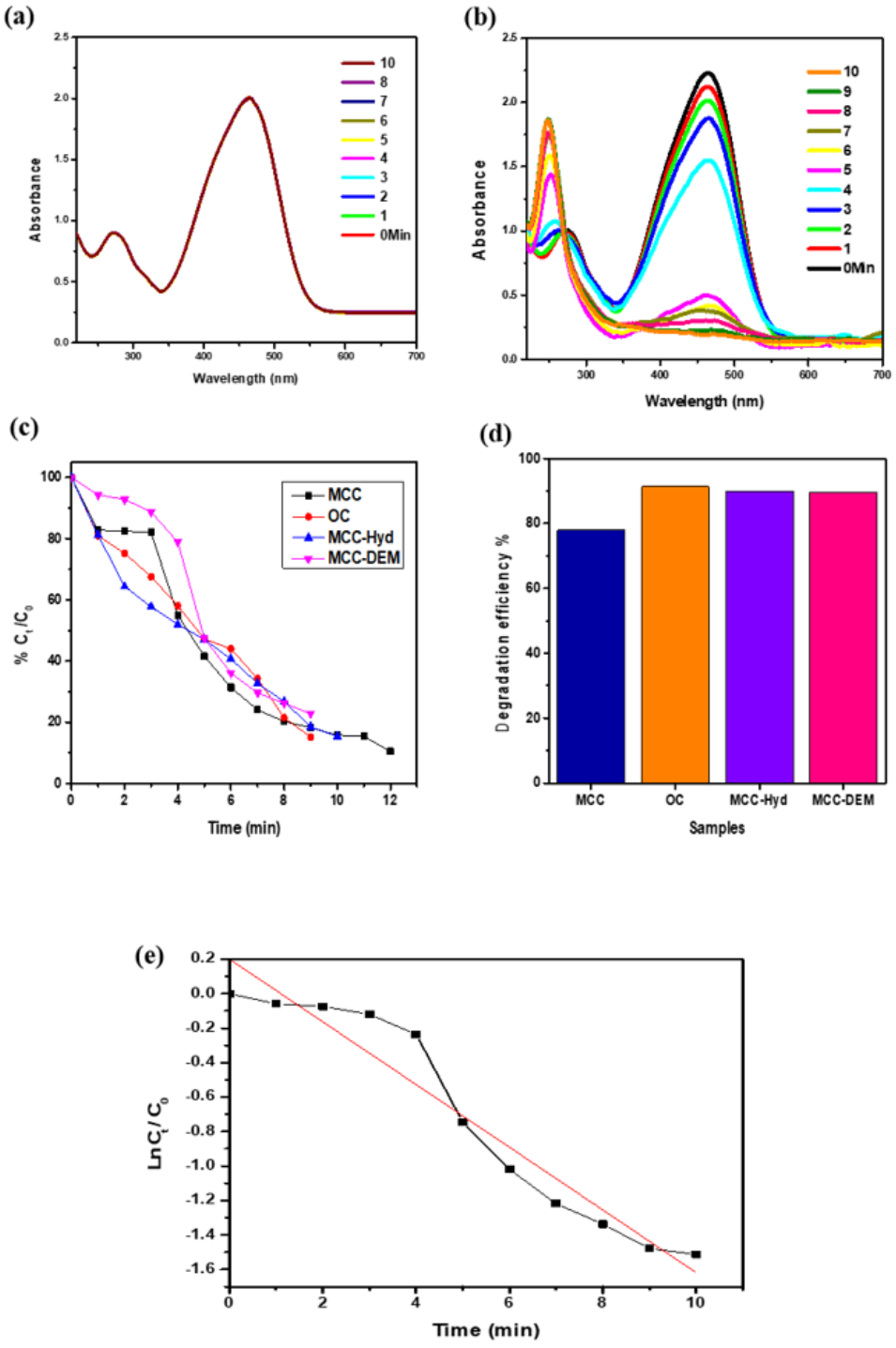

Figure 11

Absorption spectra of Methyl orange aqueous solution at different time interval. (a) Bare MCC-DEM film (b) Cu MCC-DEM film. (c) Activity of all prepared films against MO degradation. (d) Degradation efficiency of all samples against MO degradation. (e) Reaction kinetics obtained as a result of Ln Ct/C0. Experimental conditions: 0.05 Mm 2.5 mL of 4-CR, 0.5 mL NaBH4 0.5M, 1 cm strip of each film.

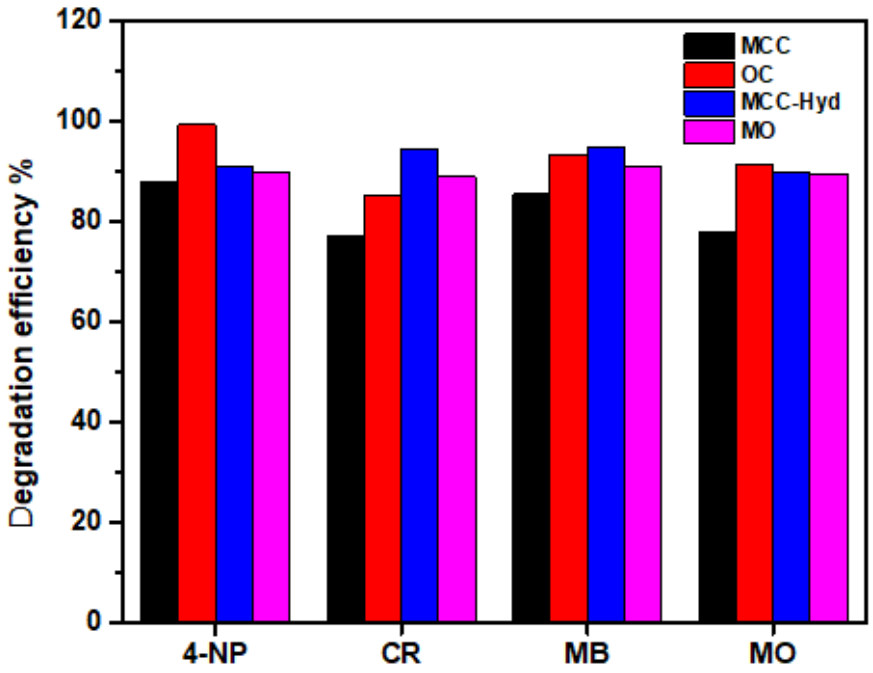

Figure 12

Comparison percentage efficiencies of all the samples against all dyes.

Supplementary Files

This is a list of supplementary files associated with this preprint. Click to download.

- GraphicalAbstract.docx